

Electronic version of an article published as *Journal of Porphyrins and Phthalocyanines*, vol. 23, no. 07/08, 2019, p. 916-929, DOI:  
[10.1142/S1088424619500809](https://doi.org/10.1142/S1088424619500809) © World Scientific Publishing Company  
<https://www.worldscientific.com/doi/pdf/10.1142/S1088424619500809>

# Supramolecular block copolymers incorporating chiral and achiral chromophores for the bottom-up assembly of nanomaterials

Marta Riba-Moliner<sup>a</sup>, Cristina Oliveras-González<sup>b</sup>, David B. Amabilino<sup>c</sup> and Arántzazu González-Campo<sup>a\*</sup>

<sup>a</sup>*Institut de Ciència de Materials de Barcelona (ICMAB-CSIC), Campus Universitari, 08193 Bellaterra, Catalonia, Spain*

<sup>b</sup>*Université d'Angers, CNRS Laboratoire MOLTECH-Anjou, UMR 6200, UFR Science, Bât. K, 2 Bd. Lavoisier, 49045 Angers, France*

<sup>c</sup>*School of Chemistry, The University of Nottingham, University Park, Nottingham, NG7 2RD, UK*

**ABSTRACT:** The coordination of the chiral metalloporphyrin ([5,10,15,20-[4-(*R,R,R*)-2-*N*-octadecylamidoethyloxiphenyl]porphyrin] zinc (II)) and an achiral homologue to an amphiphilic block copolymer of poly(styrene-*b*-4-vinyl pyridine) (PS-*b*-P4VP) have been studied in solution and as cast material. The resulting chiral dye-polymer hybrid material has been accomplished *via* axial coordination between the zinc (II) metal ion in the core of the porphyrin ring and the pyridyl units of the block-copolymer in a non-coordinative solvent. The supramolecular organization and possible chirality transfer to the hybrid material have been studied in solution by UV-vis absorption spectroscopy, fluorescence spectroscopy, Nuclear Magnetic Resonance and Circular Dichroism. The morphology of the chiral and achiral doped polymers has been studied in solid state by Transmission Electron Microscopy and Atomic Force Microscopy. We show that the nanostructures formed depend greatly upon the nature of the side-chains on the porphyrins, where a chiral group leads to a very homogeneous phase-separated material, perhaps indicating that chiral side groups are useful for the preparation of this type of supramolecular hybrid.

**KEYWORDS:** poly(styrene-*b*-4-vinyl pyridine) copolymer, chiral metalloporphyrin, doped film, micelles, hybrid material, axial coordination.

## INTRODUCTION

Synthetic supramolecular chemistry has significant potential impact in the polymer field because the properties of new hybrid materials are unique, thanks to their structures and functionalities [1]. For instance, polymer aggregation can be controlled by choosing recognition of strategic elements in macromolecular chains [2]. The

aim of the present work is to combine these features with those of  $\pi$ -functional units. Porphyrins are versatile components in supramolecular systems [3–5], and they have been studied widely due to their optical and electronic properties which make them suitable for a great variety of interests such as nanoelectronic systems [6], light-harvesting arrays [7] or dye-sensitizing chromophores in photovoltaic devices [8]. Their structural and physical properties are tuned by modifying either the side groups linked at the *meso*-position of the porphyrin ring or by chemical changes in the core, with the introduction of a metal ion in the chelating macrocycle being the simplest modification possible [9, 10]. Free-base porphyrins and

\*Correspondence to: Arántzazu González-Campo, Institut de Ciència de Materials de Barcelona (ICMAB-CSIC), Campus Universitari, 08193 Bellaterra, Catalonia, Spain, tel.: +34 935801856, e-mail: agonzalez@icmab.es.

1 metalloporphyrins can self-assemble by non-covalent  
 2 interactions [11] (such as hydrogen-bonding,  $\pi$ - $\pi$   
 3 interactions or Van der Waals forces), but the coordination  
 4 of the metal ion with an exo-facing ligand can also drive  
 5 the self-assembly of the chromophores [12]. Recently,  
 6 the ability of these metalloporphyrins to coordinate axial  
 7 groups has led to a number of novel supramolecular con-  
 8 structs that show interesting dynamic properties in the  
 9 motion of the ring [13–15].

10 At the same time, organic thin films based on amphi-  
 11 philic block copolymers (BCPs) have been deeply stud-  
 12 ied due to the tunability of the different structural patterns  
 13 adopted between the immiscible blocks at the interface  
 14 [16–19]. The volume fraction of each block and the sol-  
 15 vent used to dissolve/disperse them are the key factors to  
 16 control the type of organization adopted by the systems  
 17 [20–24]. The BCP used here is poly(styrene-*b*-4-vinyl  
 18 pyridine) (PS-*b*-P4VP), an amphiphilic macromolecule  
 19 that contains well-defined microstructures thanks to the  
 20 incompatibility of the poly(styrene) (PS) and poly(4-vinyl  
 21 pyridine) (P4VP) blocks with one another, its malleabil-  
 22 ity, pH-responsiveness and the potential reactivity, and  
 23 complex-forming ability of the P4VP block combined  
 24 with the stiffness of the PS part. The P4VP block is selec-  
 25 tively solubilized by polar protic solvents, except in water,  
 26 where it swells [25]. Conversely, the PS block is selec-  
 27 tively soluble in non-polar solvents. There are some non-  
 28 selective solvents that dissolve PS-*b*-P4VP completely,  
 29 like chloroform and tetrahydrofuran and the correspond-  
 30 ing polar-non-polar solvent mixtures. These ‘solubility  
 31 rules’ depend on the molar fraction of each block and  
 32 the degree of polymerization. Moreover, the amphiphilic  
 33 character of the BCP allows a good phase separation that  
 34 can be adjusted and to some degree induced, by controll-  
 35 ing the molar fraction and the solvent in which it is

1 partially or totally solubilized. The variety of materials  
 2 that can be achieved such as membranes, micelles and  
 3 nanostructured thin films, among others, with totally dif-  
 4 ferent final properties [26–30], together with the use of  
 5 the pyridine ring as an anchoring point have made this  
 6 BCP applicable for a wide range of systems [31–33].

7 Here, the opportunities offered by the combination of  
 8 PS-*b*-P4VP and a chiral zinc(II)-metalloporphyrin (Zn-  
 9 (*R,R,R,R*)-**1**) are explored with the ultimate aim of obtain-  
 10 ing dye-polymer hybrid materials *via* axial metal ion  
 11 coordination for potential applications in optoelectronics  
 12 [33, 34]. The zinc (II) metal ion located in the core of the  
 13 porphyrin ring will provide the possibility of coordina-  
 14 tion by the pyridyl units of the BCP, resulting in supra-  
 15 molecular self-assembled systems [35]. For this purpose,  
 16 chiral and achiral metalloporphyrins Zn-(*R,R,R,R*)-**1** and  
 17 Zn-**2** were used (Fig. 1) [36–38]. The determination of the  
 18 coordination between the PS-*b*-P4VP and the Zn porphy-  
 19 rins, as well as the possible chirality transfer to the supra-  
 20 molecular organization of the BCP with the porphyrinic  
 21 derivative compounds, will be studied in solution and in  
 22 solid state by UV-vis absorption spectroscopy (UV-vis),  
 23 Fluorescence spectroscopy and Circular Dichroism  
 24 (CD) spectroscopy. Moreover, morphological studies of  
 25 the superstructure formed by the supramolecular hybrid  
 26 will be analyzed by Transmission Electron Microscopy  
 27 (TEM) and Atomic Force Microscopy (AFM).

## 38 EXPERIMENTAL

### 39 General methods

40 **Commercially available reagents and solvents.** Styrene  
 41  $\geq 99\%$ , 4-vinyl pyridine (containing 100 ppm hydro-  
 42 quinone as inhibitor),  $\alpha$ -methylstyrene 99% (containing

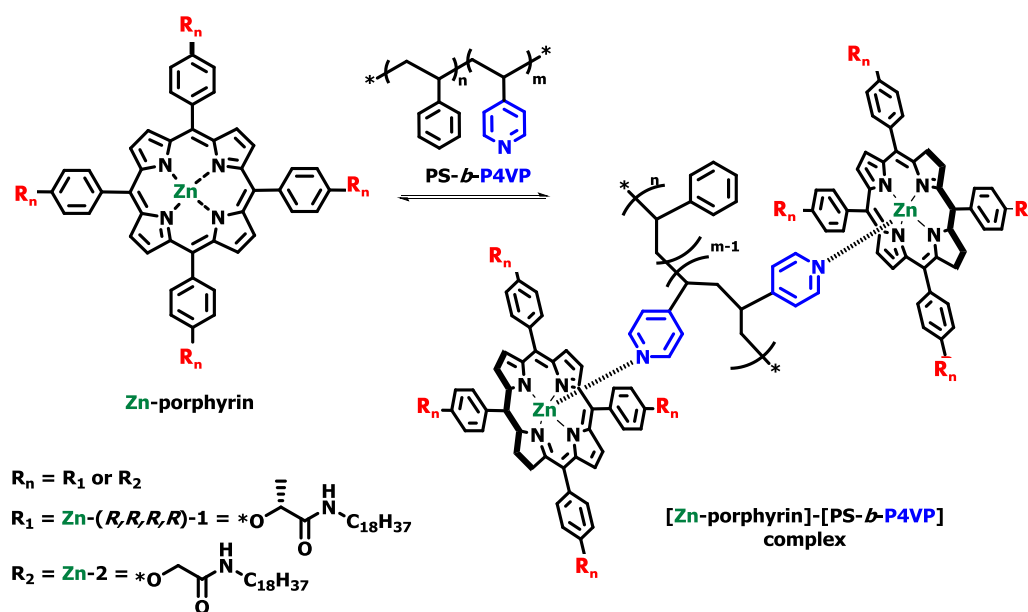


Fig. 1. Representation of the coordination of the Zn porphyrins and the PS-*b*-P4VP after their axial coordination

1 15 ppm *p*-tert-butylcatechol as inhibitor), the initiator  
2 sec-butyllithium (1.4 M in cyclohexane) and methanol  
3 (anhydrous, 99.8%) were purchased to Sigma–Aldrich.  
4 THF was HPLC degree from Teknokroma.

5 **Measurements.** UV-vis absorbance spectroscopy was  
6 measured using a Varian Cary 5000 UV-vis spectropho-  
7 tometer, in solution, with standardized quartz cuvettes of  
8 1 cm of optical path. In solid experiments, standardized  
9 quartz slides were used. Quartz surfaces were cleaned  
10 with piranha solution (H<sub>2</sub>SO<sub>4</sub>/H<sub>2</sub>O<sub>2</sub> (30%); 3:1<sub>v/v</sub>) for  
11 30 min prior to use. Nuclear Magnetic Resonance  
12 (NMR) spectra were recorded in a Bruker AVANCEII  
13 300 and Bruker Avance DRX 300 spectrometer. Matrix-  
14 Assisted Laser Desorption-Ionization Mass Spectro-  
15 metry (MALDI-TOF) measurements were performed  
16 with an Ultraflex (TOF/TOF) spectrometer. All Fourier  
17 Transform Infrared Spectroscopy (FTIR) measurements  
18 were recorded using a Perkin Elmer (Spectrum one) spec-  
19 trometer. The samples were of solid porphyrins (recov-  
20 ered after evaporation of solvent in a non-controlled  
21 precipitated way) and were performed in attenuated total  
22 reflection (ATR) mode. Porphyrins were measured on a  
23 universal ATR (UATR) plate. A Jasco J-275 spectropo-  
24 larimeter was used for Circular Dichroism (CD) spectra  
25 measurements. A Peltier-temperature programmer for  
26 thermosetting the samples was used to cool the solutions.  
27 The samples were transferred to a standardized quartz  
28 cuvette to be analyzed. When the measured temperature  
29 was reached and stabilized, spectra were recorded. Fluo-  
30 rescence spectroscopy measurements were performed  
31 using Horiba-Jobin-Yvon SPEX Nanolog-TM and Cary  
32 eclipse spectrofluorimeters. All the samples were pre-  
33 pared by diluting a solid sample of the porphyrin and  
34 BCP in the corresponding amount of solvent. Transmis-  
35 sion Electron Microscopy (TEM) images were acquired  
36 at 120 kV. TEM supports used were holey carbon coated  
37 copper grids (200 lines/inch). Only samples containing  
38 pure PS-*b*-P4VP were selectively stained with iodine  
39 vapors, and the process occurred by placing the samples  
40 in a sealed container in an iodine vapor atmosphere for  
41 1 h. 5 kV, a working distance of 10 mm, a spot of 3.5  
42 and high vacuum were the conditions used to acquire  
43 Scanning Electron Microscopy (SEM) images. Energy-  
44 dispersive X-ray spectroscopy (EDAX) was assembled to  
45 the SEM microscope with 15 kV and analyzing times of  
46 ~2500 s were the fixed conditions to collect information.

## 47 Synthesis

50 **Polymerization of PS-*b*-P4VP.** PS-*b*-P4VP (molar ratio  
51 PS:P4VP 1:4) was synthesized following the metho-  
52 dology described by Varshney *et al.* [39]. The exact  
53 procedure, amounts and volumes employed in the reaction  
54 are detailed in the Supporting Information.

55 **Synthesis of porphyrins Zn-(*R,R,R,R*)-1 and Zn-2.**  
56 [5,10,15,20-[4-(*R,R,R,R*)-2-*N*-octadecylamidoethy-  
57 loxiphenyl]porphyrin] zinc (II) (Zn-(*R,R,R,R*)-1) and

[5,10,15,20-[4-*N*-octadecylacetamidophenoxy]porphy-  
rin] zinc (II) (Zn-2) were prepared according to literature  
procedures [37, 38].

4 **Solid samples.** A dome was used to reach vacuum  
5 conditions to obtain solid samples for TEM analyses of  
6 the phase segregation and micellar aggregation.

7 **Polymeric doped micelles.** Solvent exchange method-  
8 ology: 3 mg of PS-*b*-P4VP and 0.25 mg of Zn-2 were dis-  
9 solved in 1 mL of THF. Then, 4 mL of ultrapure water was  
10 added dropwise and THF was removed from the mixture  
11 by evaporation. In parallel, the inverse process, organic-  
12 to-selective organic solvent, was also tested by preparing  
13 a solution of 3 mg of PS-*b*-P4VP and 0.25 mg of Zn-2 in  
14 THF, adding 4 mL of 1,4-dioxane dropwise and remov-  
15 ing the THF by simple evaporation. Both experiments  
16 (organic-to-selective polar and organic-to-selective  
17 organic solvents) were also performed with the chiral  
18 homologue Zn-(*R,R,R,R*)-1-based metallocompound.

## 21 RESULTS AND DISCUSSION

23 With the aim to corroborate the effectiveness of the  
24 coordination of a Zn-porphyrin with the pyridine units  
25 of the PS-*b*-P4VP (1:4), titration studies with the chiral  
26 metalloporphyrin Zn-(*R,R,R,R*)-1 and the achiral Zn-2  
27 metalloporphyrin were conducted in solution using  
28 UV-vis absorption spectroscopy [35]. Zinc (II) porphy-  
29 rins tend to bind with nitrogen axial ligands, resulting in  
30 a red-shift of the absorption bands due to an increase of  
31 the electron density of the porphyrin ring [40, 41]. First,  
32 a titration study of the Zn-(*R,R,R,R*)-1 with pyridine to  
33 form [Zn-(*R,R,R,R*)-1-(Py)] was followed by UV-vis  
34 and used as a reference (Fig. S1). The titration was  
35 carried out at room temperature using a 5 μM solution  
36 in dichloromethane of the metalloporphyrin (Sol. A)  
37 and consecutive additions of a mixed solution (Sol. B)  
38 of pyridine (1.5 mM) and Zn-(*R,R,R,R*)-1 (5 μM) in  
39 dichloromethane. After the addition of 0.15 mM of pyri-  
40 dine, a bathochromic shift of the Soret band from 423  
41 nm to 430 nm was observed. The shift of the Q<sub>α</sub> band  
42 was from 550 nm to 564 nm and, for the lower energy  
43 Q band (Q<sub>β</sub>), the shift was from 590 nm to 605 nm [40].  
44 Moreover, the Q<sub>β</sub> band showed a clear increase in rela-  
45 tive intensity with the increase of the pyridine amount.  
46 These results indicated the coordination of the pyridine  
47 with the Zinc (II) metal of the metalloporphyrin [41].  
48 Towards the complexation BCP with the metallopor-  
49 phyrins, a titration with the achiral Zn-2 porphyrin was  
50 carried out at room temperature using a 50 μM solution  
51 of the metalloporphyrin (Sol. A) in chloroform. Concur-  
52 rently, in order to avoid any dilution factor of the por-  
53 phyrin with respect to the BCP during the titration, a  
54 mixed solution composed by 47 μM of Zn-2 and 0.5 mM  
55 of BCP in chloroform was prepared (Sol. B). The UV-vis  
56 absorption analysis started with the measurement of the  
57 absorption of the metalloporphyrin solution (Sol. A)

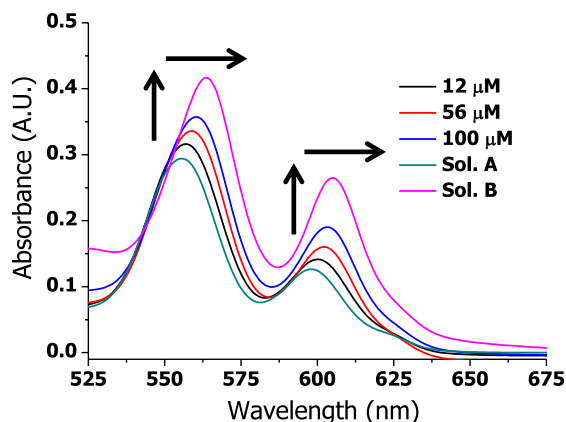
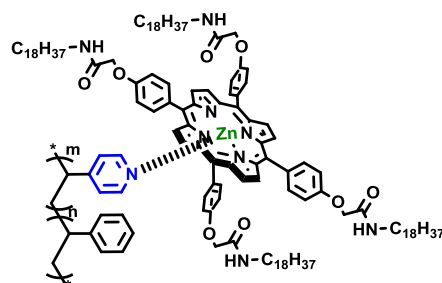


**Fig. 2.** UV-vis absorption spectra of the titration between Zn-2 (Sol. A) and Zn-2/PS-*b*-P4VP (Sol. B) to form the [Zn-2-(PS-*b*-P4VP)] complex in chloroform

and continued with consecutive additions of Sol. B (Fig. 2). In addition to the coordination between the pyridine groups of the BCP and the zinc (II) metal ion in the core of the porphyrin, Zn-2 can self-assemble by the coordination of the carbonyl group of the amide in the periphery with the zinc of an adjacent metalloporphyrin [37]. However, the non-coordinating solvent and conditions used in the titration studies avoid the self-aggregation of the metalloporphyrin to study exclusively the effects of the coordination among porphyrins and the BCP [36].

The UV-vis absorption spectra of the titration showed the progressive and characteristic evolution of the Q bands with the addition of BCP and the formation of the [Zn-2-(PS-*b*-P4VP)] complex (Fig. 2). Due to the concentrations used for the titration experiment, the signal of the Soret band was saturated and therefore, only the evolution of the Q bands was followed. The absorption band corresponding to the Q<sub>α</sub> band of the isolated Zn-2 metallocompound (Sol. A) at 556 nm increased in intensity and shifted to 564 nm with the increase of the of PS-*b*-P4VP concentration. Similarly, the Q<sub>β</sub> band experienced a bathochromic shift from 598 nm to 605 nm when the binding to PS-*b*-P4VP occurred. The observed changes confirmed the axial coordination between the zinc (II) metal ion of the Zn-2 and the nitrogen of the pyridine in solution, and therefore the formation of the [Zn-2-(PS-*b*-P4VP)] complex [35, 41]. The solution containing the complex was drop-cast on a quartz slide, and the film remaining after evaporation of the solvent was analyzed by UV-vis absorption spectroscopy. The spectrum of the film showed a similar bathochromic shift of the Q<sub>α</sub> and Q<sub>β</sub> bands to the complex in solution (in both cases, 11 nm) with respect to the pure Zn-2 solution (Fig. S2). These results showed the viability of casting the complex for the preparation of films of [Zn-2-(PS-*b*-P4VP)].

The formation of the complex between the chiral metalloporphyrin Zn-(*R,R,R,R*)-1 and the BCP was also proven both in solution and upon drop-casting onto



quartz (Figs S3 and S4) by the red shift of the Q bands of the porphyrin. In solution, two isosbestic points appeared at 534 nm and at 588 nm in the UV-vis absorption spectra (Fig. S3). As a film, the complex showed a similar absorption spectrum to the achiral complex (Fig. S4).

Fluorescence spectroscopic measurements of the metalloporphyrins and their complexes also confirmed the formation of the supramolecular polymer. The spectra of the chiral metalloporphyrin and its complex with the BCP showed emission from the first excited state (*S*<sub>1</sub>) to the ground state (*S*<sub>0</sub>) upon excitation at 551 nm and 601 nm for metalloporphyrin Zn-(*R,R,R,R*)-1 and 554 nm and 601 nm for the complex [Zn-(*R,R,R,R*)-1-(PS-*b*-P4VP)], respectively (Fig. 3). The emission of the porphyrin in the complex was also red-shifted compared to the free compound. The Q<sub>β</sub> band presented a larger Stokes shift (62 nm) for the [Zn-(*R,R,R,R*)-1-(PS-*b*-P4VP)] complex than for the isolated metalloporphyrin Zn-(*R,R,R,R*)-1 (55 nm), due to the electron-donating character of the pyridyl group [42, 43].

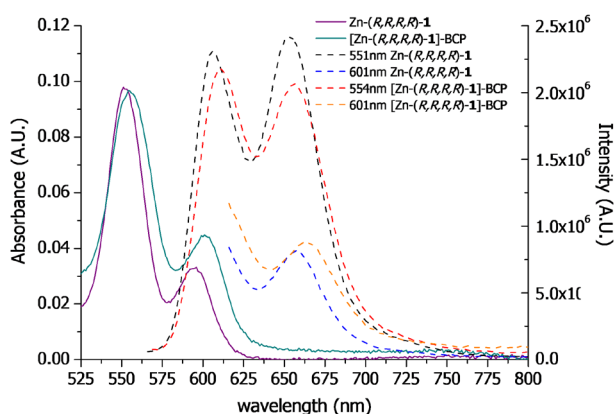


**Fig. 3.** UV-vis absorption and fluorescence spectra of Zn-(*R,R,R,R*)-1 (5 μM) and [Zn-(*R,R,R,R*)-1-(PS-*b*-P4VP)] complex (5 μM) in chloroform solution

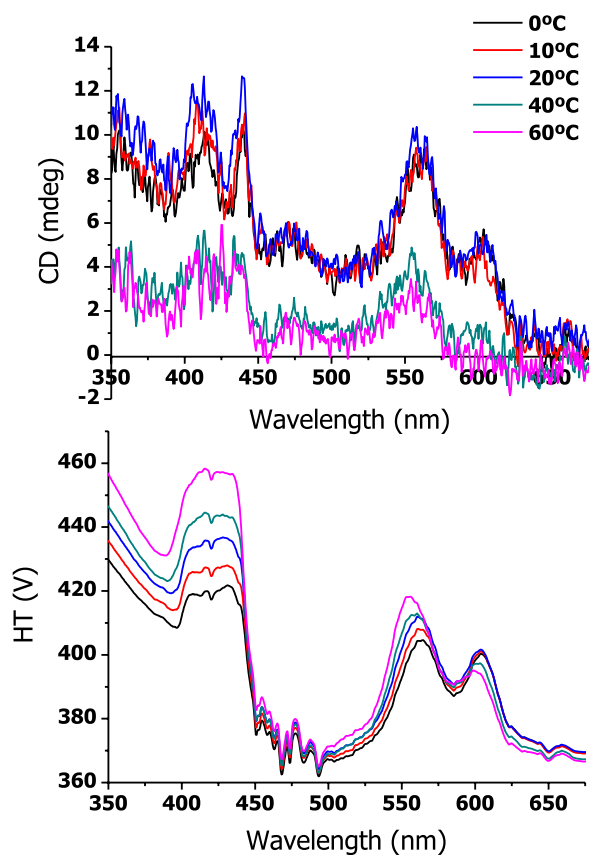


**Fig. 4.** CD and corresponding and the corresponding absorption spectra of [Zn-(*R,R,R,R*)-1-(PS-*b*-P4VP)] complex in chloroform solution (50  $\mu$ M) within the temperature range 0  $^{\circ}$ C to 60  $^{\circ}$ C. HT(V) means High Tension (Voltage)

The chirality present in the side-chains of Zn-(*R,R,R,R*)-1 could, in principle, lead to a chiral amplification, which could be observed through an increase of the optical activity of Zn-(*R,R,R,R*)-1-(PS-*b*-P4VP)] complex [12, 13, 44, 45]. Circular Dichroism (CD) spectroscopy is an extremely sensitivity probe for supramolecular structures [46]. Therefore, any proximity of porphyrin groups coordinated along the P4VP block should be detected using the technique. The complex was analyzed within a temperature range from 0  $^{\circ}$ C to 60  $^{\circ}$ C (Fig. 4). The CD spectra showed a slight temperature-dependence behavior of the Zn-(*R,R,R,R*)-1-(PS-*b*-P4VP)] complex, being more evidence in the Q bands in the corresponding absorption spectra. From 0  $^{\circ}$ C to 20  $^{\circ}$ C, clear CD signals were observed in the region of the Soret band and especially in the Q band area. The intensity of these signals was very low (a few millidegrees), which is characteristic of chromophores in a chiral environment that is dominated by the stereochemistry point rather than chiral order between chromophores (which is, generally, much more intense) [47]. With the increase of the temperature, a significant decrease in the optical activity, together with a slight blue shift of the Q-bands absorption were observed, suggesting a possible de-coordination of

the pyridyl units of the BCP and the zinc (II) metal ion of the porphyrin. On the other hand, CD studies of the film of the [Zn-(*R,R,R,R*)-1-(PS-*b*-P4VP)] complex on quartz gave only a noisy and low intensity CD signal response (Fig. S5). This result indicated that the transmission of chirality from the stereogenic centers to the porphyrin organization was not effective in the complexes, where the average local achiral complex formation dominates. It should be pointed out that the pyridyl units can be occur locally chiral positions, although the atactic nature of the polymer meant that a regular interaction between porphyrins coordinated to the same chain was not possible.

$^1$ H NMR experiments were also performed consecutively in solution to assess the binding between the metalloporphyrin and the BCP. Solutions of Zn-(*R,R,R,R*)-1, [Zn-(*R,R,R,R*)-1-(PS-*b*-P4VP)] complex and pure PS-*b*-P4VP in deuterated chloroform were studied at 298 K (Fig. S6). Some differences between the [Zn-(*R,R,R,R*)-1-(PS-*b*-P4VP)] complex and the PS-*b*-P4VP spectra were observed (Fig. S6). A slight shift and a broadening of the peaks positioned at 6.4 and 8.3 ppm were experienced after the coordination. These peaks correspond to the protons of pyridine groups of the BCP, whose changes were in concordance with the expected results [35, 48]. Furthermore, the peak at 8.9 ppm for Zn-(*R,R,R,R*)-1 shifted down to 8.7 ppm when the porphyrin was coordinated, which corresponds to the protons of the pyrrole rings.

#### **Morphology of [Zn-2-(PS-*b*-P4VP)] and [Zn-(*R,R,R,R*)-1-(PS-*b*-P4VP)] complexes**

The organization of the [Zn-2-(PS-*b*-P4VP)] and [Zn-(*R,R,R,R*)-1-(PS-*b*-P4VP)] complexes at the microscopic level as materials was studied by Atomic Force Microscopy (AFM) (see Supporting information for sample preparation). The topography AFM images of [Zn-2-(PS-*b*-P4VP)] (Figs 5a–5d) and [Zn-(*R,R,R,R*)-1-(PS-*b*-P4VP)] (Figs 5e–5h) showed apparently quite different morphology at larger length scales (several microns). The achiral complex depicted a quite flat surface with apparent very thin flake-like features and larger solid particle-like features protruding from the surface (Figs 5a–5d). On the other hand, the complex incorporating the chiral porphyrin evidenced a very regular morphology, where flake-like objects (about 0.5  $\mu$ m in width and 1–3  $\mu$ m in length) were arranged randomly over the surface (Figs 5e–5h). Closer inspection of the surface (Fig. 5f) showed small round objects of approximately 20 nm high and 100 nm wide (Fig. 5h) localized between the flakes, which appeared rough but had no well-defined structure.

These features contrasted with those observed for the pure Zn-(*R,R,R,R*)-1, which arranged to form forming rounded dot-like features (average diameter of 0.5  $\mu$ m) (Fig. S7). This relevant difference in the packing highlighted the influence of incorporating the BCP in the self-assembly phenomenon of the complex. The morphology

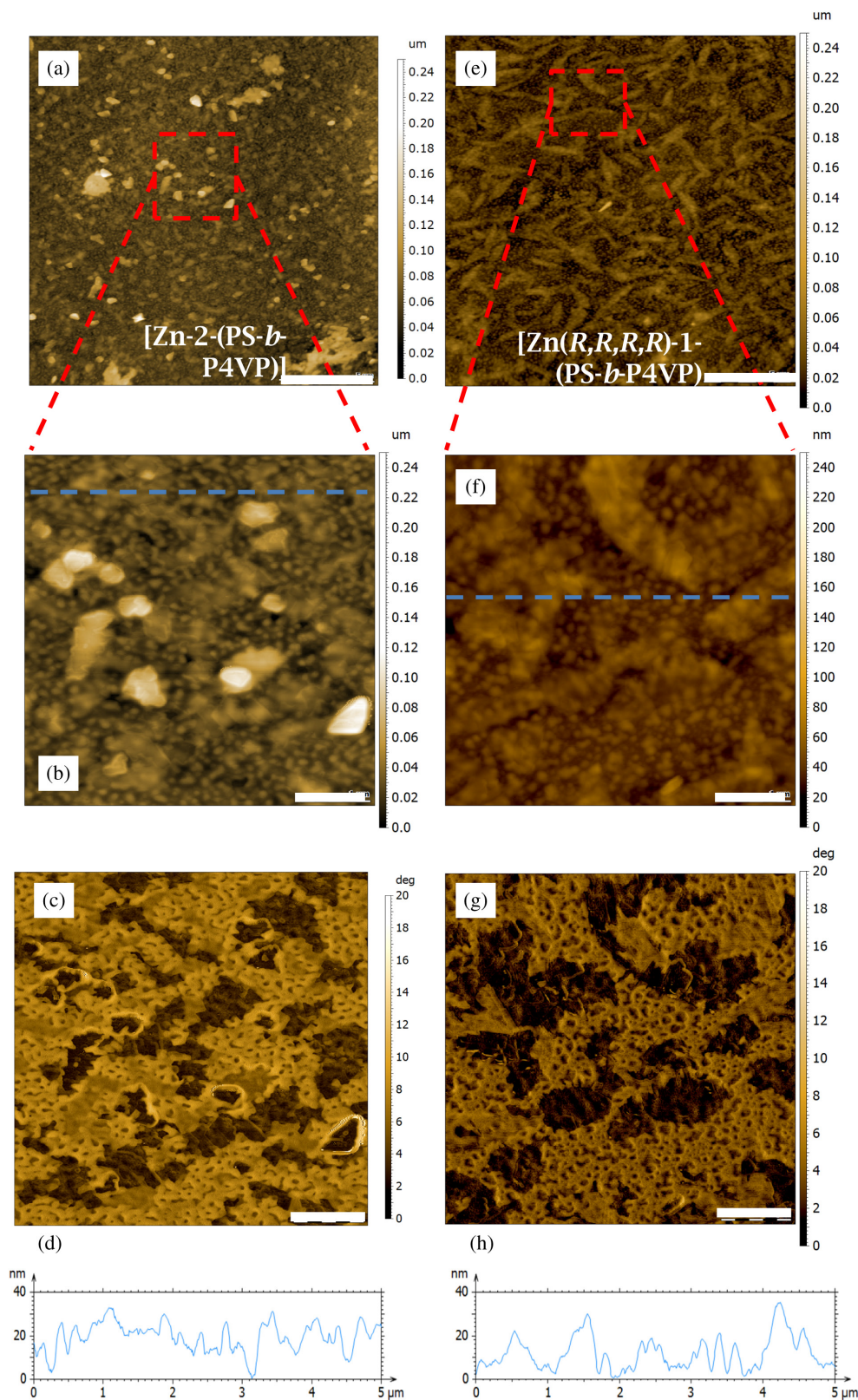
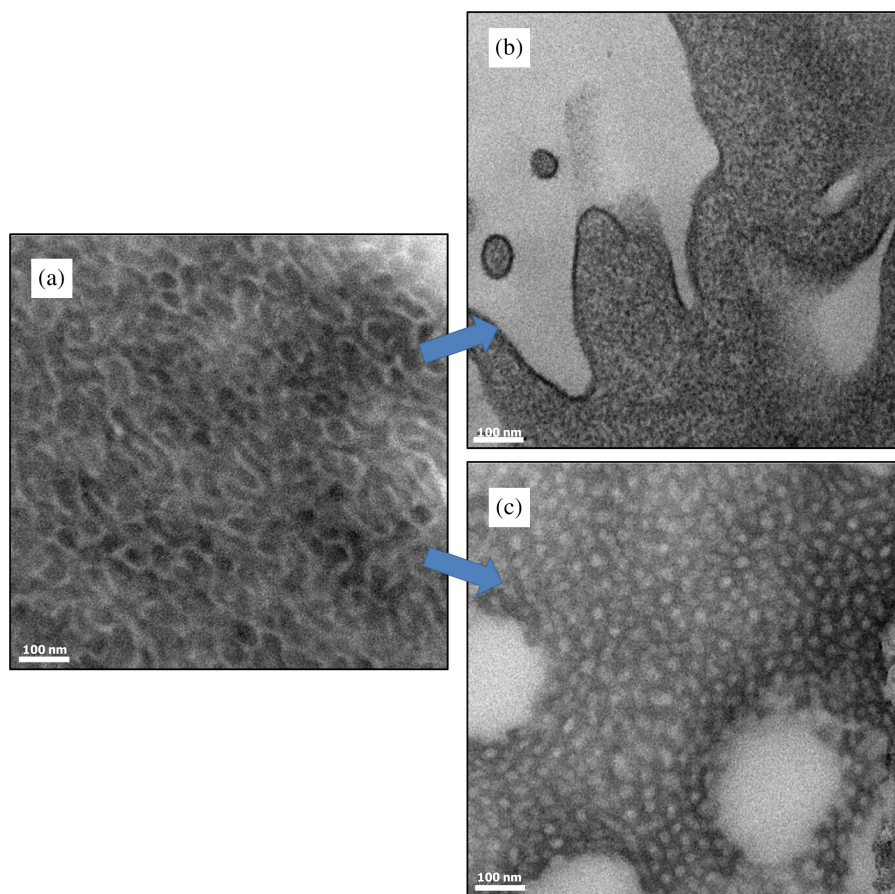


**Fig. 5.** AFM images of [Zn-2-(PS-*b*-P4VP)] (a–d) and [Zn(*R,R,R,R*)-1-(PS-*b*-P4VP)] (e–h) coordinated compounds from a solution of chloroform drop-casted on HOPG surfaces. Topography images are shown in a and e (scale bars indicate 5  $\mu\text{m}$ ), b and f are closer-up topographic images from a and e (indicated with red dashed lines). Blue dashed lines indicate where the height profiles were taken from (scale bars indicate 1  $\mu\text{m}$ ), and c and g are phase images corresponding to topographic images b and f (scale bars indicate 1  $\mu\text{m}$ ). Height profiles corresponding to the horizontal dashed lines in b, f are shown in d and h

1 of the achiral complex exhibited similar nanometer-scale  
2 round features with the previously mentioned larger particles overlaid (Fig. 5d). These larger particles, which  
3 appeared crystalline, were presumably the small molecules (since they were not present in the other complex)  
4 and were dark in the phase image from the AFM (Fig. 5c).  
5 In this phase image, the higher flake-like regions also  
6 appeared dark, indicating that they corresponded to the porphyrin component as well. In between these dark  
7 areas, quite well-defined nanostructured regions with  
8 dark dots were spotted, corresponding with the 20-nm-  
9 tall dots, in both the achiral and chiral samples. There-  
10 fore, the nanostructure of the material was similar in both  
11 cases, although it was more homogeneous in the case of  
12 the chiral porphyrin complex. These images contrasted  
13 with AFM images of pure PS-*b*-P4VP, prepared under  
14 same conditions (Fig. S8). The AFM topography of PS-*b*-  
15 P4VP (Fig. S8a) showed an irregular holed layer, proba-  
16 bly as a consequence of the free evaporation of the solvent  
17 that created inhomogeneities during the evaporation, and  
18 consequently left locally dewetted regions. When the  
19 layer was analyzed closely, phase segregation from the  
20 continuous layer of the polymer was observed, although  
21 the holes were too large to obtain better contrasted  
22  
23  
24  
25  
26  
27  
28  
29  
30  
31  
32  
33  
34  
35  
36  
37  
38  
39  
40  
41  
42  
43  
44  
45  
46  
47  
48  
49  
50  
51  
52  
53  
54  
55

images (Fig. S8b). As a consequence of the large holes,  
not much information could be extracted from the phase  
image (Fig. S8c). In summary, both, height profiles of  
the achiral and chiral metalloporphyrin-based complexes  
exhibited flake-like structures of ~35 nm in height and  
small spherical-shaped objects with averaged diameters  
of ~50 nm and ~100 nm in [Zn-2-(PS-*b*-P4VP)] and [Zn-  
(*R,R,R,R*)-1-(PS-*b*-P4VP)], respectively (Figs 5d and 5h).  
Contrarily, the size of the objects observed in the pure  
polymer was ~10 nm (Fig. S8d).

Transmission Electron Microscopy (TEM) was used  
to determine the influence of the chirality of the meta-  
lloporphyrins in the phase segregation of the complexes.  
Separate solutions of PS-*b*-P4VP, [Zn-2-(PS-*b*-P4VP)]  
and [Zn-(*R,R,R,R*)-1-(PS-*b*-P4VP)] in chloroform were  
dried under vacuum for several hours until solid pow-  
ders were afforded. The final powders were separately  
embedded in an epoxy resin and cured at 60 °C for 2  
days. Then, they were cut by using a microtome to finally  
obtain solid films with a thickness of 70–100 nm. The  
different samples were collected on holey-carbon copper  
TEM grids and were also selectively stained with iodine  
vapors for 1 h in a sealed container. TEM images of the  
pure block copolymer showed phase segregation with



56 **Fig. 6.** TEM images of (a) the pure PS-*b*-P4VP, and the porphyrin complexes (b) [Zn-2-(PS-*b*-P4VP)] and (c) [Zn-(*R,R,R,R*)-1-(PS-  
57 *b*-P4VP)], obtained by microtoming solid samples from a dried chloroform solution (Scale bars indicate 100 nm)



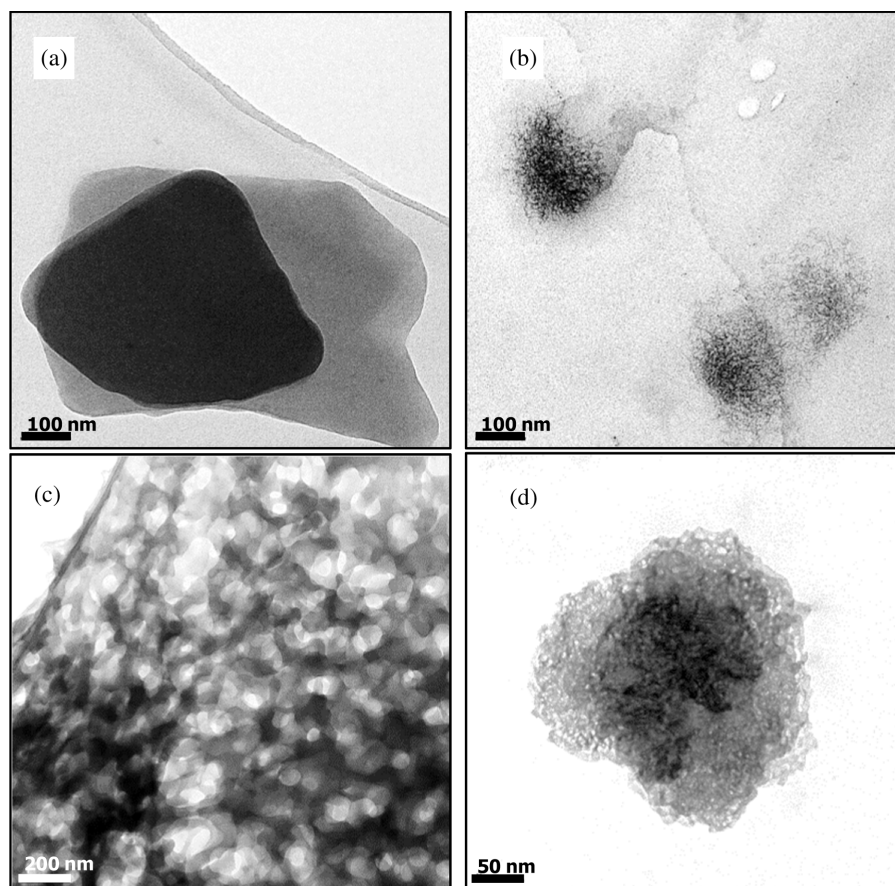


**Fig. 7.** TEM images of Zn-porphyrins and their complexes with PS-*b*-P4VP obtained from solutions in ethanol by drop-casting on carbon coated copper (a) Zn-**2** (scale bar indicates 100 nm), (b) Zn-(*R,R,R,R*)-**1** (scale bar indicates 100 nm), (c) [Zn-**2**-(PS-*b*-P4VP)] (scale bar indicates 200 nm), (d) [Zn-(*R,R,R,R*)-**1**-(PS-*b*-P4VP)] (scale bar indicates 50 nm)

a quasi-lamellar structure with darker domains corresponding to the P4VP block (as a consequence of the staining used to enhance TEM contrast) (Fig. 6a). The [Zn-**2**-(PS-*b*-P4VP)] complex showed an unclear order (Fig. 6b). However, [Zn-(*R,R,R,R*)-**1**-(PS-*b*-P4VP)] chiral complex displayed very defined domains, dark areas with bright spots, probably arranging either in body-centered cubic spheres (fm3m), gyroid (ia3d) or inverse discontinuous cubic structure (fd3m) (Fig. 6c). This evidence proved the effect of the presence of stereogenic centers in the alkyl chains of the porphyrin chains on the self-assembly of the supramolecular PS-*b*-P4VP complex, resulting in segregated regions with different structures. The chiral characteristic, given only by a single methyl group in each substituted alkyl chain, enlarged significantly the space domains between PS and P4VP, probably because of the higher steric hindrance between neighboring metalloporphyrin units anchored to the pyridyl groups.

While the coordination of the porphyrin to the BCP in the composite material is clear, an alternative assembly strategy to obtain nanostructured materials was studied by modifying the polarity of solvents to obtain polymeric doped micelles [49–51]. Li and coworkers reported chiral

core-shell micelles based on the electrostatic interactions between poly(ethylene glycol)-*b*-poly(4-vinyl pyridine) block copolymer and achiral free-based tetrakis(4-sulfonatophenyl) porphyrin [52]. Therefore, the complex formation using purely coordinative bonds in different solvents was explored. As starting point, 0.04 mM solutions of Zn-**2** and Zn-(*R,R,R,R*)-**1** and a dispersion (0.02 mM) of PS-*b*-P4VP in ethanol were prepared. Then, 1 mL of each solution of Zn-**2** or Zn-(*R,R,R,R*)-**1** were mixed with 1 mL of PS-*b*-P4VP dispersion, respectively. Pure and mixed porphyrin-based solutions were drop-cast on carbon coated copper TEM grids for further analysis. The TEM measurements of Zn-**2** (Fig. 7a) revealed solid plate-like objects formed by the porphyrins, with approximate diameters of 650 nm. The coordination of Zn-**2** to PS-*b*-P4VP (Fig. 7c) resulted in an apparently porous network. In this unstained sample, the darker regions were presumably P4VP-Zn-**2**, similar to the observations of Yao *et al.* in aggregated chiral compounds with achiral polymers [53]. On the other hand, TEM images of the chiral porphyrin Zn-(*R,R,R,R*)-**1** (Fig. 7b) evidenced a less dense material, even though some slice-like parts (less compact than the achiral porphyrin) were observed. More aggregated fibrous coiled elements were obtained

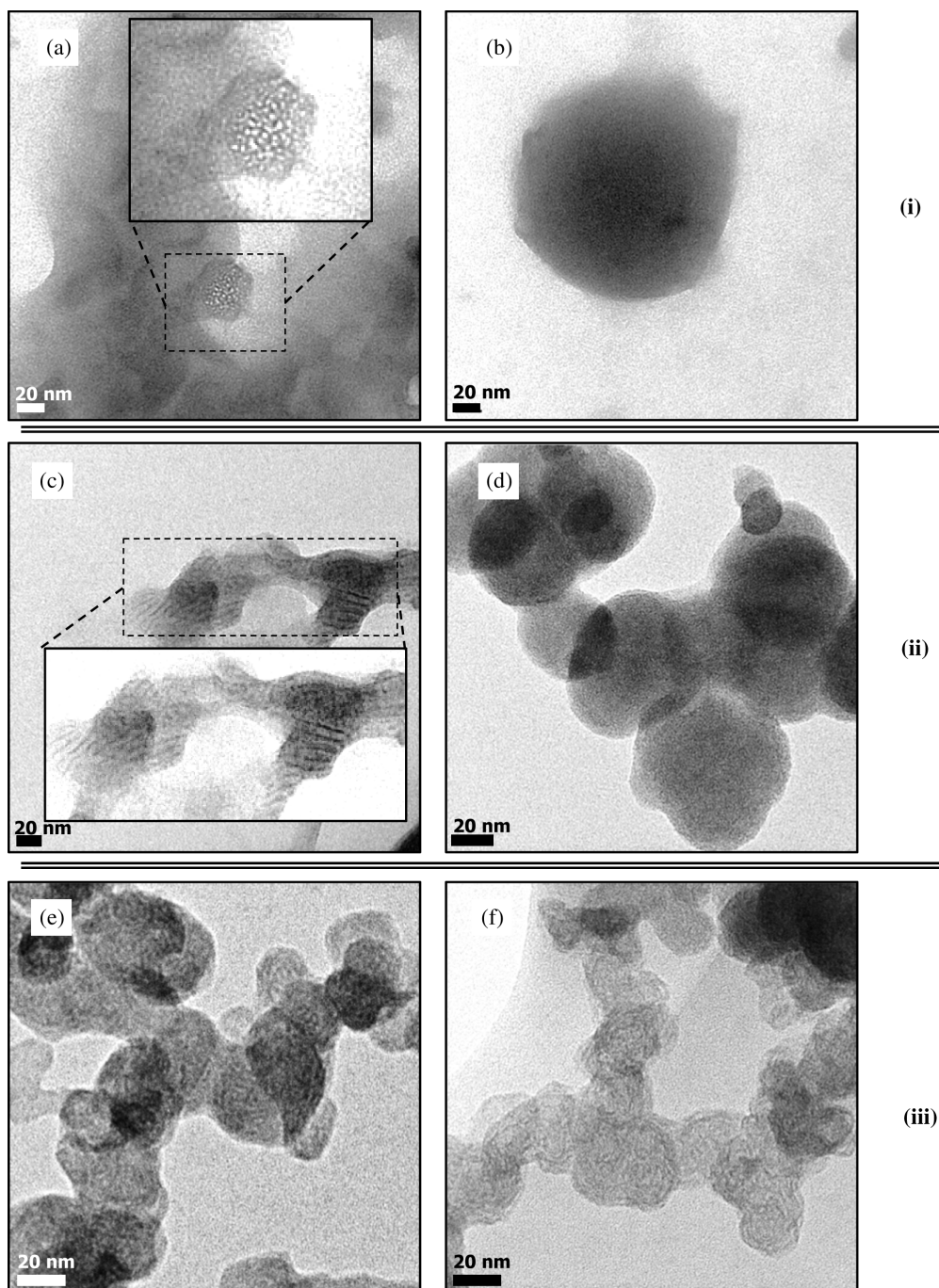


**Fig. 8.** TEM images of [Zn-(*R,R,R,R*)-1-(PS-*b*-P4VP)] samples prepared from ethanol. (a) and (b) from a drop of the mixed solution without staining, (c) and (d) from the dried mixed solution embedded in an epoxy resin without staining and, (e) and (f) from dried mixed solution embedded in an epoxy resin stained with I<sub>2</sub> vapors (Scale bars indicate 20 nm)

than in Zn-2. In the [Zn-(*R,R,R,R*)-1-(PS-*b*-P4VP)] complex (Fig. 7d), well-defined “cauliflower”-shaped structures were observed. A significantly more fibrous structure at the corona of the “flowers” suggested that polymer coiled with Zn-(*R,R,R,R*)-1, leading to twisted fibrous meshes.

To further study the [Zn-(*R,R,R,R*)-1-(PS-*b*-P4VP)] complex morphology in ethanol, different preparation methodologies of the TEM samples were tested: (i) a drop

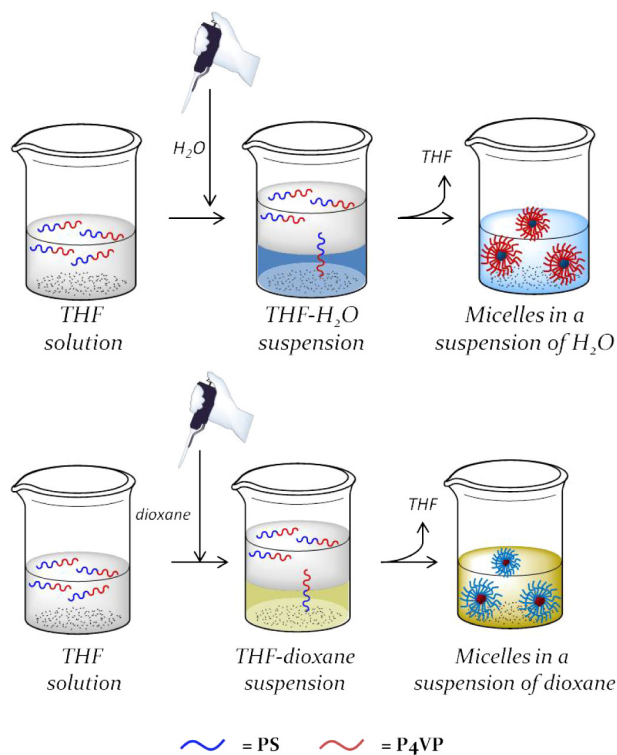
of solution was cast on a holey-carbon copper TEM grid and directly analyzed, (ii) an aliquot of the solution was dried and then was embedded in an epoxy resin, the resin was cured and then, cut using microtome in thin slices (70–100 nm) and analyzed by TEM without staining, and (iii) the same procedure as (ii) but the sample was stained with I<sub>2</sub> vapors for 1 h in a sealed container before TEM imaging (Fig. 8). All the samples indicated similar superstructures, albeit with varying degrees of detail (Fig. 8).

From the drop of the solution of the [Zn-(*R,R,R,R*)-1-(PS-*b*-P4VP)] complex analyzed directly by TEM (Figs 8a–8b), some regions with agglomerated matter and spherical aggregates with blurred perimeter were appreciated. The majority of the round objects were small, but within a broad range of sizes (from 40 to 300 nm). The more continuous film seen in Fig. 8a indicated a twisted-layer type structure. When the sample was prepared with epoxy resin, self-assembled Zn-(*R,R,R,R*)-1 porphyrin domains became clearly visible in the continuous-type structure (Fig. 8c), and the aggregated particles were spotted, although no internal structure was evident (Fig. 8d). The dark regions in Fig. 8c probably corresponded to regions containing Zn-(*R,R,R,R*)-1 porphyrin, forming stripes of 4 nm of separation, because the sample was not selectively stained. After enhancing the contrast by selectively staining the P4VP domains with  $I_2$  vapors, the distribution of the BCP in the [Zn-(*R,R,R,R*)-1-(PS-*b*-P4VP)] micelles could be clearly appreciated as layers of ~4 nm of material (Figs 8e–8f). Images illustrated a possible twisted rope-like structure which could belong to P4VP domains, possibly coiled by the chiral effect of the porphyrin, although no handedness could be determined from the images.

With the aim to elucidate if the self-assembled complex in the corona of micelles in ethanol, corresponding to the [Zn-(*R,R,R,R*)-1-(PS-*b*-P4VP)] complex, was optically active, CD measurements of the micelles in solution were performed (Fig. S9). However, no indication of chiral packing was observed, suggesting that no chiral chromophore interaction was present in the materials, and consequently, no significant chiral superstructure could be evidenced.

An alternative way to form the complex between the porphyrin and the BCP is by the solvent exchange methodology [54, 55]. The solvent exchange procedure involves, first, dissolving the amphiphilic copolymer in a non-selective solvent and, secondly, slowly adding a selective solvent until the latter is in excess. Then the non-selective solvent is removed (usually by evaporation), leading to a solvent exchange. In principle, progressive evaporation of the non-selective component induced the collapse of the solvophobic part of the copolymer, leading to a micelle-like structure (Scheme 1). To prove this, organic-to-selective polar solvent exchange was tested in the present systems.

PS-*b*-P4VP and the corresponding Zn-2 or Zn-(*R,R,R,R*)-1 porphyrin were dissolved in THF, ultrapure water was added dropwise and THF was removed from the mixture by evaporation. In parallel, the inverse process, organic-to-selective organic solvent, was also tested by the preparation of a solution of PS-*b*-P4VP and Zn-2 or Zn-(*R,R,R,R*)-1 in THF, addition of 1,4-dioxane dropwise and removal of the THF by simple evaporation. Additionally, control experiments for each solvent exchange process with pure PS-*b*-P4VP, Zn-2 and Zn-(*R,R,R,R*)-1 under the same conditions



**Scheme 1.** Representation of the formation of the PS-*b*-P4VP micelles depending on the polarity of the solvent (solvent exchange method)

and following the same procedures were performed. A drop of each final mixture was separately analyzed by TEM using holey-carbon copper grids. TEM images of PS-*b*-P4VP in water (Fig. S10) revealed well-defined round micelle-like objects with a narrow range of sizes (~150–400 nm). The P4VP phase was selectively stained with iodine vapors, appearing as dark regions. Klinger *et al.* observed similar micelles of PS-*b*-P2VP following a similar procedure [56]. When the solvent inducing the micellar assembly was 1,4-dioxane, a core of P4VP surrounded by a PS corona was expected [57]. TEM images of this sample showed smaller micellar structures than in water which were surrounded by poorly defined matter (blurry appearance) (Fig. S11). After staining, the P4VP domains appeared spherical (darker regions in the images) surrounded by the PS block, probably swollen as a result of the contact with 1,4-dioxane, and consequently, forming blurred matter in their surroundings [58]. The volume fraction of the blocks in the PS-*b*-P4VP used here (molar ratio PS:P4VP of 1:4) surely determined sizes, distributions and behavior of micelle-like objects in the different solvents studied, due to the selectivity of each block. The TEM image of pure Zn-2 in water showed straight, planar and large ribbon morphologies (Fig. S11a) [59]. However, when 1,4-dioxane was used, Zn-2 precipitated (Fig. S11b), forming mixed structures, plates (as

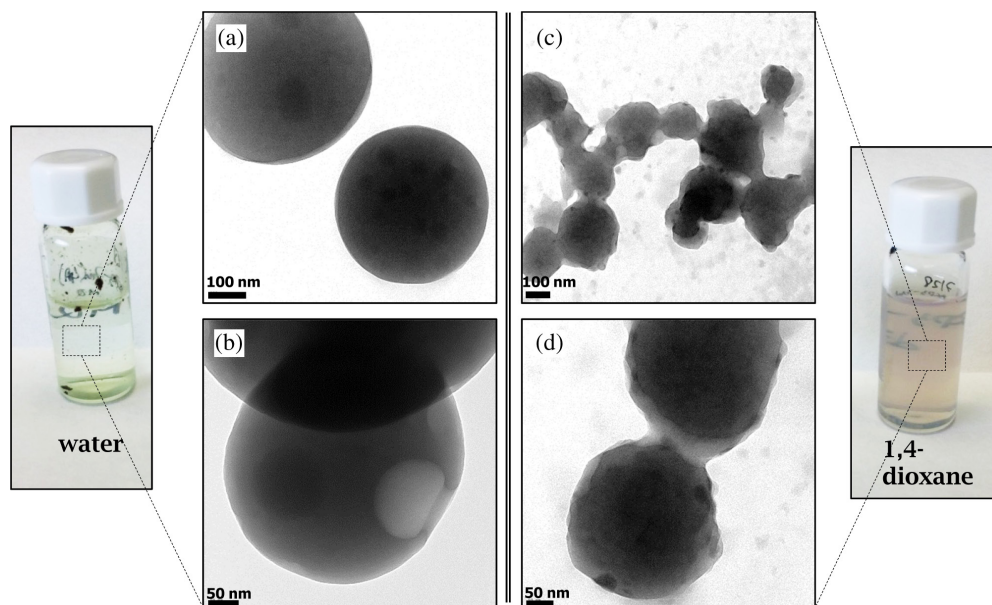


**Fig. 9.** Pictures of [Zn-2-(PS-*b*-P4VP)] solutions in water (greenish) and in 1,4-dioxane (pale rose). TEM images of [Zn-2-(PS-*b*-P4VP)] micelles in water (a) and (b) and in 1,4-dioxane (c) and (d) (a and c scale bars indicate 100 nm; b and d scale bars indicate 50 nm)

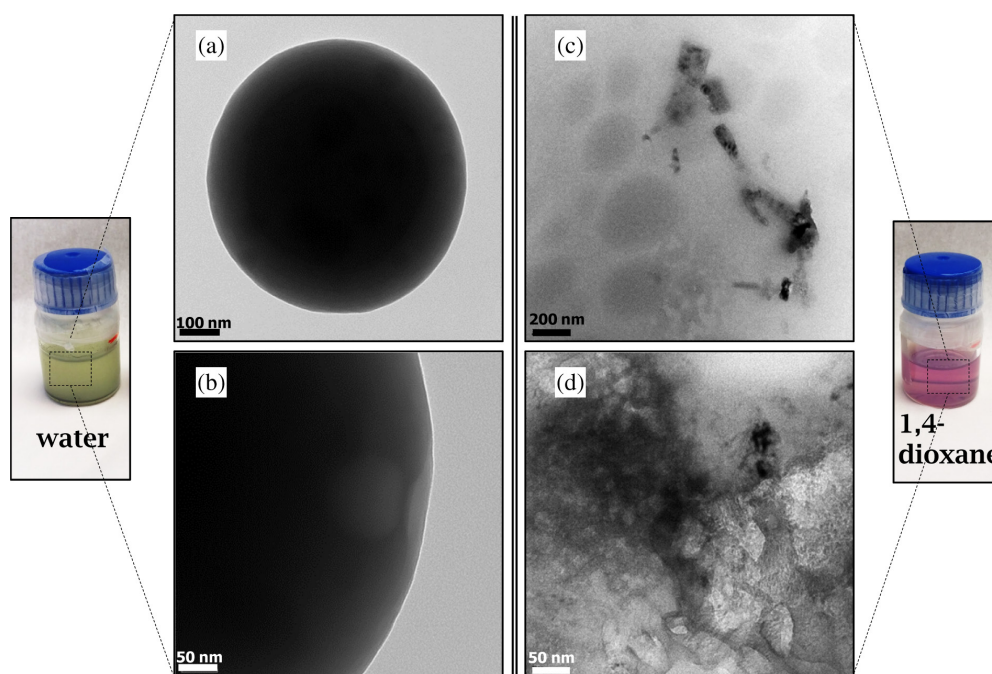


**Fig. 10.** Pictures of [Zn-(*R,R,R,R*)-1-(PS-*b*-P4VP)] solutions in water (greenish) and 1,4-dioxane (pink) and TEM images of: (a) and (b) [Zn-(*R,R,R,R*)-1-(PS-*b*-P4VP)] micelles in water and, (c) and (d) [Zn-(*R,R,R,R*)-1-(PS-*b*-P4VP)] mixed compound in 1,4-dioxane (a scale bar indicates 100 nm; b scale bar indicates 50 nm; c scale bar indicates 200 nm; d scale bar indicates 50 nm)

observed from ethanol) as well as wider ribbons due to the coordinative character of the solvent [60]. Moreover, TEM images of the chiral Zn-(*R,R,R,R*)-1 precipitated in water (Fig. S11c) depicted very small round aggregates (sub-20 nm) with barely discernible fibrous substructures, very different from the achiral homologue.

When the solvent was 1,4-dioxane (Fig. S11d), similar aggregates to those in water were found, although with a larger surface (approximately 80 nm) with internal fibrous nanostructures.

On the other hand, TEM images of [Zn-2-(PS-*b*-P4VP)] formed very well-defined round and filled

spheres (Figs 9a–9d). While in water and after THF evaporation, the spheres had a diameter of approximately 500 nm (Figs 9a–9b); from the 1,4-dioxane mixture, the spheres had diameters between 200 and 300 nm, with a rougher appearance (Figs 9c–9d). In both samples, darker spots were also seen inside the spheres, probably due to enriched porphyrin localized areas. For the sample prepared in water, in which the hydrophilic pyridyl fragments seems to be in contact with the water, unlike the organic solvent exchange, rougher and smaller particles with clear coronas (presumably composed of PS domains) were observed (Figs 9a–9b). An increased tendency towards aggregation between the particles in 1,4-dioxane was appreciated, due to the affinity between alkyl chains of neighboring packed porphyrins that could be swelled by the organic solvent (Figs 9c–9d).

The chiral complex [Zn-(*R,R,R,R*)-**1**-(PS-*b*-P4VP)] also formed well-defined particles in water, approximately 500 nm in diameter (Figs 10a–10b), similar to its achiral homologue. In contrast, when the chiral metallo-compound was immersed in 1,4-dioxane (Figs 10c–10d), no particulate aggregation was observed, and only polymer phase segregation and aggregates could be discerned (Fig. 10c). Apparently, no coordination between the PS-*b*-P4VP and Zn-(*R,R,R,R*)-**1** was concluded, and coordination of the zinc (II) with the 1,4-dioxane occurred [60]. This fact was assumed because of the higher solubility of the chiral porphyrin in contrast to the achiral one, and the large excess of solvent used compared to the polymer amount. Snitka *et al.* observed similar striped structures (they designated them as molecular ribbons) in aggregates of tetrakis(4-sulfonatophenyl)porphyrin, supporting the coordination of the precursors by the solvent [61].

## CONCLUSIONS

The binding of both achiral and chiral zinc (II) porphyrins to the pyridyl block of the polymer is clear both in solution in a non-coordinating solvent (chloroform) and in films. The system can also be used to make nanomaterials whose morphology depends on the chiral or non-chiral form of the coordinated zinc (II) porphyrin analogue. The coordinated systems [Zn-**2**-(PS-*b*-P4VP)] and [Zn-(*R,R,R,R*)-**1**-(PS-*b*-P4VP)] have differences in their morphology as cast materials, observing more uniformity for the chiral complex as well as when precipitation under far-from-equilibrium conditions occurred. Notably, the precipitation in water generates the most homogeneous material although no well-defined substructure exists in the particle generated. The chiral complex does not show significant optical activity either in solution or in the nanomaterials prepared, indicating that the polymer coordination prevents the proximity of the chromophores and stereogenic centers. This situation contrasts dramatically from the situation in which the pure porphyrins stack on top of one another thanks to

hydrogen bonding, leading to significant optical activity. It also indicates that this kind of polymer with an atactic and rigid structure in combination with the necessary axial coordination of the pyridine groups and the chiral zinc (II) porphyrins is not suited. Therefore, a block copolymer with a control of the tacticity and phase segregation will be more appropriate for further studies of chirality transfer in this kind of dye-polymer hybrid material.

## Acknowledgements

We thank T. Parella (UAB) for help in DOSY-NMR measurements, J. Oró (ICMAB) for help in TEM imaging and M. Simón (ICMAB) for help in AFM imaging. The work was supported by MINECO with the Project MAT2016-77852-C2-1-R (AEI/FEDER, UE) and MAT2013-47869-C4-2-P and Generalitat de Catalunya for the project 2017-SGR-1277. AGC acknowledges financial support from the Spanish Ministry of Economy and Competitiveness through the “Severo Ochoa” Programme for Centres of Excellence in R&D (SEV- 2015-0496) and the Ministry of Science, Innovation and Universities for a Ramon y Cajal contract (RYC-2017-22910).

## Supporting information

Additional information on coordination studies and synthesis and characterization studies, including Figs. S1–S11 are available are given in the supplementary material. This material is available free of charge *via* the Internet at <http://www.worldscinet.com/jpp/jpp.shtml>.

## REFERENCES

1. Harada A. *Supramolecular Polymer Chemistry*, Wiley-VCH Verlag GmbH & Co. KGaA: Weinheim, Germany, 2011.
2. Thibault RJ and Rotello VM. In *Molecular Recognition and Polymers*, John Wiley & Sons, Inc., Hoboken, NJ, 2008; 1–7.
3. Elemans JAAW, Van Hameren R, Nolte RJM and Rowan AE. *Adv. Mater.* 2006; **18**: 1251–1266.
4. Yan Q, Luo Z, Cai K, Ma Y and Zhao D. *Chem. Soc. Rev.* 2014; **43**: 4199–4221.
5. Zhang C, Chen P, Dong H, Zhen Y, Liu M and Hu W. *Adv. Mater.* 2015; **27**: 5379–5387.
6. Aragonès AC, Darwish N, Saletta WJ, Pérez-García L, Sanz F, Puigmartí-Luis J, Amabilino DB and Díez-Pérez I. *Nano Lett.* 2014; **14**: 4751–4756.
7. Imahori H. *J. Phys. Chem. B.* 2004; **108**: 6130–6143.
8. Louahem M’Sabah B, Boucharef M, Warnan J, Pellegrin Y, Blart E, Lucas B, Odobel F and Boucle J. *Phys. Chem. Chem. Phys.* 2015; **17**: 9910–9918.
9. Goldberg I. *Chem. Comm.* 2005; **10**: 1243–1254.
10. Chmielewski PJ and Latos-Grażyński L. *Coord. Chem. Rev.* 2005; **249**: 2510–2533.

- 1 11. Pasternack RF, Giannetto A, Pagano P and Gibbs 1
- 2 EJ. *J. Am. Chem. Soc.* 1991; **113**: 7799–7800. 2
- 3 12. Beletskaya I, Tyurin VS, Tsvadze AY, Guillard R 3
- 4 and Stern C. *Chem. Rev.* 2009; **109**: 1659–1713. 4
- 5 13. Ogi S, Ikeda T, Wakabayashi R, Shinkai S and 5
- 6 Takeuchi M. *Chem. — Eur. J.* 2010; **16**: 8285–8290. 6
- 7 14. Sguerra F, Bulach V and Hosseini MW. *Dalton* 7
- 8 *Trans.* 2012; **41**: 14683–14689. 8
- 9 15. Puigmarti-Luis J, Salettra WJ, Gonzalez A, Amabi- 9
- 10 lino DB and Pérez-García L. *Chem. Comm.* 2014; 10
- 11 **50**: 82–84. 11
- 12 16. Hamley IW. *Prog. Polym. Sci.* 2009; **34**: 1161–1210. 12
- 13 17. Kim JK, Yang SY, Lee Y and Kim Y. *Prog. Polym.* 13
- 14 *Sci.* 2010; **35**: 1325–1349. 14
- 15 18. Heier J, Kramer EJ, Walheim S and Krausch G. 15
- 16 *Macromolecules* 1997; **30**: 6610–6614. 16
- 17 19. Albert JNL and Epps III TH. *Mater. Today* 2010; 17
- 18 **13**: 24–33. 18
- 19 20. Bates FS and Fredrickson GH. *Phys. Today* 1999; 19
- 20 **52**: 32–38. 20
- 21 21. Gowd EB, Böhme M, Stamm M. *IOP C. Ser. Mater.* 21
- 22 *Sci. Eng.* 2010; **14**: 012015. 22
- 23 22. Sinturel C, Vayer M, Morris M and Hillmyer MA. 23
- 24 *Macromolecules* 2013; **46**: 5399–5415. 24
- 25 23. Kao J, Thorkelsson K, Bai P, Rancatore BJ and Xu 25
- 26 T. *Chem. Soc. Rev.* 2013; **42**: 2654–2678. 26
- 27 24. Gowd EB, Koga T, Endoh MK, Kumar KV and 27
- 28 Stamm M. *Soft Matter* 2014; **10**: 7753–7761. 28
- 29 25. D’Aprano A and Fuoss RM. *J. Polym. Sci.* 1969; **7**: 29
- 30 1101–1109. 30
- 31 26. Letchford K and Burt H. *Eur. J. Pharm. Biopharm.* 31
- 32 2007; **65**: 259–269. 32
- 33 27. Li X and Han Y. *J. Mater. Chem.* 2011; **21**: 33
- 34 18024–18033. 34
- 35 28. Radjabian M, Koll J, Buhr K, Handge UA and 35
- 36 Abetz V. *Polymer* 2013; **54**: 1803–1812. 36
- 37 29. Clodt JI, Filiz V, Rangou S, Buhr K, Abetz C, Höche 37
- 38 D, Hahn J, Jung A and Abetz V. *Adv. Funct. Mater.* 38
- 39 2013; **23**: 731–738. 39
- 40 30. Klinger D, Wang CX, Connal LA, Audus DJ, Jang 40
- 41 SG, Kraemer S, Killops KL, Fredrickson GH, 41
- 42 Kramer EJ and Hawker CJ. *Angew. Chem., Int. Ed.* 42
- 43 2014; **53**: 7018–7022. 43
- 44 31. Bronstein LM, Sidorov SN, Valetsky PM, Hartmann 44
- 45 J, Cölfen H and Antonietti M. *Langmuir* 1999; **15**: 45
- 46 6256–6262. 46
- 47 32. Guldi DM, Rahman GM, Qin S, Tchoul M, Ford 47
- 48 WT, Marcaccio M, Paolucci D, Paolucci F, Cam- 48
- 49 pidelli S and Prato M. *Chem. — Eur. J.* 2006; **12**: 49
- 50 2152–2161. 50
- 51 33. Arulkashmir A, Mahale RY, Dharmapurikar SS, 51
- 52 Jangid MK and Krishnamoorthy K. *Polym. Chem.* 52
- 53 2012; **3**: 1641–1646. 53
- 54 34. Huang HX, Liu J and Cai YQ. *J. Lumin.* 2013; **143**: 54
- 55 447–452. 55
- 56 35. Gao B, Wang R and Du R. *J. Porphyrins Phthalocyanines* 2010; **14**: 235–243. 56
- 57 36. Oliveras-González C, Di Meo F, González-Campo 57
- A, Beljonne D, Norman P, Simón-Sorbed M, 1
- Linares M and Amabilino DB. *J. Am. Chem. Soc.* 2
- 2015; **137**: 15795–15808. 3
37. Feldborg LN, Salettra WJ, Iavicoli P and Amabi- 4
- lino DB. *J. Porphyrins Phthalocyanines* 2011; **15**: 5
- 995–1003. 6
38. Iavicoli P, Xu H, Feldborg LN, Linares M, Paradi- 7
- nas M, Stafström S, Ocal C, Nieto-Ortega B, 8
- Casado J, López Navarrete JT, Lazzaroni R, Feyter 9
- SD and Amabilino DB. *J. Am. Chem. Soc.* 2010; 10
- 132**: 9350–9362. 11
39. Varshney SK, Zhong XF and Eisenberg A. *Macro-* 12
- molecules* 1993; **26**: 701–706. 13
40. Gautam R and Chauhan SMS. *Mater. Sci. Eng. C* 14
- Mater.* 2014; **43**: 447–457. 15
41. Alessio E. *Structure and Bonds: Non-Covalent* 16
- Multi-Porphyrin Assemblies: Synthesis and Proper-* 17
- ties*, Springer, 2006; Vol. 121, pp. 1–47. 18
42. Apanasovich VV, Novikov EG, Yatskov NN, Koe- 19
- horst RBM, Schaafsma TJ and van Hoek A. *J. Appl.* 20
- Spectrosc.* 1999; **66**: 613–616. 21
43. Karolczak J, Kowalska D, Lukaszewicz A, 22
- Maciejewski A and Steer RP. *J. Phys. Chem. A* 23
- 2004; **108**: 4570–4575. 24
44. Green MM, Reidy MP, Johnson RD, Darling G, 25
- O’Leary DJ and Willson G. *J. Am. Chem. Soc.* 26
- 1989; **111**: 6452–6454. 27
45. Palmans ARA and Meijer EW. *Angew. Chem., Int.* 28
- Ed.* 2007; **46**: 8948–8968. 29
46. Gottarelli G, Lena S, Masiero S, Pieraccini S and 30
- Spada GP. *Chirality* 2008; **20**: 471–485. 31
47. Pescitelli G, Di Bari L and Berova N. *Chem. Soc.* 32
- Rev.* 2014; **43**: 5211–5233. 33
48. Pale V, Nikkonen T, Vapaavuori J, Kostianien M, 34
- Kavakka J, Selin J, Tittonen I and Helaja J. *J. Mater.* 35
- Chem. C* 2013; **1**: 2166–2173. 36
49. Štěpánek M, Matějček P, Humpolíčková J, 37
- Havránková J, Podhájecká K, Špírková M, Tuzar Z, 38
- Tsitsilianis C and Procházka K. *Polymer* 2005; **46**: 39
- 10493–10505. 40
50. Fan H and Jin Z, *Soft Matter* 2014; **10**: 2848–2855. 41
51. Connal LA, Lynd NA, Robb MJ, See KA, Jang SG, 42
- Spruell JM and Hawker CJ. *Chem. Mater.* 2012; **24**: 43
- 4036–4042. 44
52. Li J, An Y, Chen X, Xiong DA, Li Y, Huang N and Shi 45
- L. *Macromol. Rapid Commun.* 2008; **29**: 214–218. 46
53. Yao L, Lu X, Chen S and Watkins JJ. *Macromol-* 47
- ecules* 2014; **47**: 6547–6553. 48
54. Robb MJ, Connal LA, Lee BF, Lynd NA and 49
- Hawker CJ. *Polym. Chem.* 2012; **3**: 1618–1628. 50
55. Krogstad DV, Lynd NA, Choi SH, Spruell JM, 51
- Hawker CJ, Kramer EJ and Tirrell MV. *Macromol-* 52
- ecules* 2013; **46**: 1512–1518. 53
56. Klinger D, Robb MJ, Spruell JM, Lynd NA, 54
- Hawker CJ and Connal LA. *Polym. Chem.* 2013; **4**: 55
- 5038–5042. 56
- 57

1	57. Bharatiya B, Schumers JM, Poggi E and Gohy JF.	60. Mikhalitsyna EA, Tyurin VS, Nefedov SE, Syrbu	1
2	<i>Polymers</i> 2013; <b>5</b> : 679–695.	SA, Semeikin AS, Koifman OI and Beletskaya IP.	2
3	58. Nunes SP, Karunakaran M, Pradeep N, Behzad AR,	<i>Eur. J. Inorg. Chem.</i> 2012; <b>12</b> : 5979–5990.	3
4	Hooghan B, Sougrat R, He H and Peinemann KV.	61. Snitka V, Rackaitis M and Rodaite R. <i>Sens. Actua-</i>	4
5	<i>Langmuir</i> 2011; <b>27</b> : 10184–10190.	<i>tors, B</i> 2005; <b>109</b> : 159–166.	5
6	59. Ogi S, Sugiyasu K, Manna S, Samitsu S and Takeu-		6
7	chi M. <i>Nat. Chem.</i> 2014; <b>6</b> : 188–195.		7
8			8
9			9
10			10
11			11
12			12
13			13
14			14
15			15
16			16
17			17
18			18
19			19
20			20
21			21
22			22
23			23
24			24
25			25
26			26
27			27
28			28
29			29
30			30
31			31
32			32
33			33
34			34
35			35
36			36
37			37
38			38
39			39
40			40
41			41
42			42
43			43
44			44
45			45
46			46
47			47
48			48
49			49
50			50
51			51
52			52
53			53
54			54
55			55
56			56
57			57